Electrokinetic and hydrodynamic properties of charged-particles systems: From small electrolyte ions to large colloids

G. Nägele,[1,*] M. Heinen,[2] A.J. Banchio,[3] and C. Contreras - Aburto[4]

[1] *Institute of Complex Systems (ICS-3), Research Centre Jülich, 52425 Jülich, Germany,*
[2] *Institut für Theoretische Physik II, Weiche Materie, Heinrich-Heine-Universität Düsseldorf, 40225 Düsseldorf, Germany*
[3] *FaMAF, Universidad Nacional de Córdoba, and IFEG-CONICET, Ciudad Universitaria, X5000HUA Córdoba, Argentina*
[4] *División de Ciencias e Ingenierías, Universidad de Guanajuato Campus León, 37150 León, México*

Dynamic processes in dispersions of charged spherical particles are of importance both in fundamental science, and in technical and bio-medical applications. There exists a large variety of charged-particles systems, ranging from nanometer-sized electrolyte ions to micron-sized charge-stabilized colloids. We review recent advances in theoretical methods for the calculation of linear transport coefficients in concentrated particulate systems, with the focus on hydrodynamic interactions and electrokinetic effects. Considered transport properties are the dispersion viscosity, self- and collective diffusion coefficients, sedimentation coefficients, and electrophoretic mobilities and conductivities of ionic particle species in an external electric field. Advances by our group are also discussed, including a novel mode-coupling-theory method for conduction-diffusion and viscoelastic properties of strong electrolyte solutions. Furthermore, results are presented for dispersions of solvent-permeable particles, and particles with non-zero hydrodynamic surface slip. The concentration-dependent swelling of ionic microgels is discussed, as well as a far-reaching dynamic scaling behavior relating colloidal long- to short-time dynamics.

I. INTRODUCTION

Dispersions of charged globular particles undergoing correlated Brownian motions are ubiquitously found with a broad range of particle sizes, ranging from electrolyte solutions through solutions of nanometer-sized globular proteins to dispersions of micron-sized charge-stabilized colloidal spheres.

Charge-stabilized colloid particles are encountered in a rich variety in chemical industry, biology and food science. Composite and aspherical colloidal particles have attracted increasing attention in soft matter science. These classes of colloids include suspensions of rods, discs, core-shell particles with a solid core and surrounding polyelectrolyte brush layer, star polymers and ionic microgels, to name only a few examples. The stimuli-dependent size and biocompatibility of microgels such as poly (N-isopropylacrylamide) (PNiPAm) allows for their use in biomedical applications including drug delivery. Experimentally well-studied examples of globular proteins are, e.g., bovine serum albumin (BSA), lyzoyzme, and apoferritin [1–6]. If dispersed in water, the proteins are moderately charged, by an amount depending on temperature, pH value, salinity, and protein concentration. A quantitative understanding of the dynamics in concentrated solutions of interacting proteins is of importance, e.g., to the evaluation of cellular functions. Conduction-diffusion and viscoelastic transport coefficients of electrolyte solutions are of relevance in electrochemistry, geology, energy research, and biology [7, 8]. They play an important role in many industrial processes including waste water treatment and ion exchange applications. A thorough theoretical understanding of electrolyte transport properties of non-dilute solutions has still not been achieved, in spite of the large body of accumulated empirical data [9, 10].

While on first sight electrolyte ions, globular proteins and spherical charged colloids appear to be very different, from a simplifying theoretical viewpoint they can be all treated as (uniformly) charged Brownian spheres, interacting by Coulomb plus excluded volume forces, and immersed in a structureless Newtonian solvent characterized by the dielectric constant ϵ and the shear viscosity η_0. In this primitive model (PM) type picture, the dynamics of all ionic species, i.e. colloid and protein macroions as well as electrolyte microions, is taken to be overdamped, with the configurational evolution of all ions described by the many-particle generalized Smoluchowski equation (GSmE) in combination with the low-Reynolds number creeping flow equation for the solvent. Such a simplifying description makes good sense also for electrolyte solutions [11], even though ion-solvent specific effects on the molecular level [12], commonly addressed using concepts such as hydration shells, local solvent polarization by ion electric fields, and structure-breaking and structure-making ion properties, are *per se* not accounted for in the PM-GSmE model. However, ion hydration shells can be approximately accounted for in a structureless solvent model by using mixed slip-stick hydrodynamic boundary conditions (BCs) on the PM microion surfaces, and by allowing for a certain solvent permeability.

The dynamics of macroions and microions is determined by the interplay of direct electrosteric forces

* g.naegele@fz-juelich.de

and indirect, solvent-mediated hydrodynamic interactions (HIs). The latter are long-ranged and in general of many-body nature [13]. This causes challenging problems in theoretical and computer simulation studies of Brownian ion systems. The dynamics of colloidal macroions much larger than electrolyte and surface-released counterions is therefore frequently described using the one-component macroion fluid model (OMF). In this simplifying model, only the microion-dressed colloidal particles are considered which interact for non-overlap distances by an effective screened Coulomb pair potential. The averaged microion degrees of freedom enter into the OMF description only through effective colloidal charge number and electrostatic screening parameters, which in general are dependent on the thermodynamic state. The simplicity of the OMF allows for a quantitative consideration of the strong colloid-colloid HIs in dense charge stabilized suspensions. However, it disregards electrokinetic effects on the colloid dynamics, arising in particular from the non-instantaneous dynamic response, to internal or external perturbations, of the microion cloud surrounding each colloidal macroion. This so-called microion relaxation mechanism is most influential for low colloid concentrations and smaller macroion sizes, and when the Debye effective screening length is comparable to the macroion radius. An additional electrokinetic mechanism of purely hydrodynamic origin becomes operative when an electric field is applied (electrophoresis). This so-called electrophoretic mechanism describes the slowing influence on the field-induced macroion migration owing to the hydrodynamic coupling with surrounding counter- and coions.

Colloidal electrokinetic effects have been studied in the past mainly using the standard electrokinetic theory (SET) approach where the microions are described as continuous local charge densities coupled to the solvent creeping flow, with advection-diffusion type Nernst-Planck constitutive equations for the microion fluxes [14, 15]. The SET equations are commonly linearized with respect to the driving field. In this mean-field type approach, microion correlations are disregarded which are important when the macroions are small such as in the case of proteins, or when the macroions are strongly charged and non-monovalent counterions are present. Microion correlation effects have been included approximately in recent extensions of the SET equations [16–19]. In the extension by Lozada-Cassou and collaborators [20–22], microion finite sizes are incorporated through a non-ideal contribution to the microionic electrochemical potential, evaluated to first order in the external electric field using the hybrid HNC-MSA equilibrium ionic pair distribution functions for a restricted PM electrolyte surrounding a spherical macroion. The macroion zeta potential at the slipping surface is identified with the equilibrium mean electrostatic potential at the closest approach distance to the microion (see also [23]). A possible sign reversal of the electrophoretic mobility is hereby directly linked to a corresponding colloidal charge reversal. In the approach by Lozada-Cassou *et al.*, the microions are dynamically still treated as continuous charge density fields. The reduced screening ability of non-zero-sized microions reduces the relaxation effect, giving rise to an enlarged macroion electrophoretic mobility at large zeta potential values.

While developed originally for a single colloidal particle in an electrolyte solution, the SET approach has been extended over the years to concentrated suspensions, mostly on basis of simplifying cell models [14, 24–34]. These cell model SET extensions, although being quite successful in predicting general trends in electrophoresis and sedimentation, are of an *ad hoc* nature and do not properly account for macroion-macroion correlations arising from overlapping colloidal electric double layers (EDLs) and colloid-colloid HIs. This is also reflected in the still ongoing discussion about the appropriate electric and hydrodynamic BCs at the outer cell boundary (see, e.g. [35]). The SET cell models predict the electrophoretic mobility to decrease in general with increasing volume fraction, also for low-polar solvents [36], and with increasing overlap of the colloidal EDLs. In most calculations, either a constant surface potential or surface charge density have been assumed, but chemically charge-regulated colloidal surfaces are also considered [37]. Moreover, cell model dc and ac electrophoretic calculations for core-shell spheres with microion-penetrable shells have been made [38, 39].

There exist also two-colloid extensions of the SET approach which have been used, e.g., for determining the concentration dependence of the electrophoretic mobility in semi-dilute suspensions [40–42]. This two-colloid approach gives in particular the correct solvent backflow factor $\left[1 - 1.5\,\phi + \mathcal{O}\left(\phi^2\right)\right]$ with the colloid volume fraction ϕ, multiplying the single-colloid Smoluchowski electrophoretic mobility of monodisperse and non-conducting colloidal spheres with ultrathin EDLs. The electrophoretic mobility and the flow behavior of suspensions of interacting colloidal charged spheres can be determined from the measured power spectrum using low-angle super-heterodyne Doppler velocimetry. Experimental results by this method, and an outline of the underlying light scattering theory, are given in [43].

We point out that different from colloidal systems, all ions in electrolyte solutions are of comparable size, charge, and mobility. Therefore, a full PM-GSmE description of the microion electrokinetics is required for non-dilute systems with all ions treated individually as dynamic entities.

In this work, we review recent advances in the theoretical understanding of linear diffusion-convection and rheological transport properties characterizing dispersions of globular charged Brownian particles. The review encompasses a broad range of properties, including microionic conductivities and electrophoretic mobilities, high-frequency and steady-state viscosities, generalized sedimentation coefficients, and self- and collective diffusion coefficients.

Theoretical methods for the calculation of conduction-diffusion coefficients and the viscosity of strong electrolyte solutions are reviewed in Sec. II. The section includes new results which we have obtained using a simplified mode-coupling theory (MCT) method where ion-ion HIs are properly accounted for not only in the short-time response, but also in the microion clouds relaxation contribution. In Sec. III, the dynamics in solutions of globular proteins is addressed. We demonstrate that theoretical methods developed originally for colloids can be successfully applied to crowded protein solutions such as BSA. Sec. IV reports on recent progress in the understanding of transport properties of concentrated suspensions of charge-stabilized colloidal particles. In particular, the dynamic behavior of solvent-permeable particles, and of ionic microgels penetrable by surrounding counterions is discussed. Our conclusions are contained in Sec. V. A list of abbreviations is included following the acknowledgements.

II. ELECTROLYTE SOLUTIONS

We consider here strong electrolyte solutions where the salt solute is fully dissociated. At total electrolyte concentrations n_T lower than about 0.01 M, electrolyte ions can be treated as pointlike, and their Coulomb interactions give rise to the peculiar square-root in concentration dependence of electrolyte transport properties. This concentration dependence is the hallmark of the Debye-Falkenhagen-Onsager-Fuoss (DFOF) limiting law expressions for the transport coefficients characterizing electrolyte conductivity and electrophoresis [44, 45], self-diffusion [46], and viscosity [44, 45, 47]. The limiting law expressions have been derived using a continuum model for the solvent, with the ions treated as pointlike Brownian particles described by equilibrium pair distribution functions on the linear Debye-Hückel (DH) theory level.

Various routes have been followed in the past for calculating conduction-diffusion and rheological properties of non-dilute electrolytes where the excluded volume of the ions needs to be considered. Falkenhagen [12] and Ebeling *et al.* [48, 49] have extended the DFOF continuity equations approach to finite ion sizes. The relaxation mechanism contribution to the conductivity is deduced in their approach from averaging the electrostatic force experienced by a central ion using the perturbed ionic pair distribution functions.

A considerable improvement over the DFOF theory was obtained by Bernard, Turq, Blum, Dufreche and collaborators in a series of publications [50–54] where the DFOF approach has been combined (mostly) with the analytic mean-spherical approximation (MSA) solution [55, 56] for the ionic pair distribution functions. They obtained results for the steady-state ion conductivity [50, 52, 54], the ion self-diffusion coefficients [57], and the mutual (chemical) diffusion coefficient [58, 59] (see also [60, 61]). The in general non-negligible influence of the ion-ion HIs on the ion cloud relaxation mechanism is disregarded in their treatment, except for the special case of ionic self-diffusion [62]. Moreover, the electrolyte viscosity has not been considered in their works

In recent works, Chandra, Bagchi and collaborators have combined MCT and dynamic density functional theory (DDFT) arguments to derive expressions for the molar conductivity [53, 63, 64] and viscosity [65] of electrolyte solutions. The ion excluded volumes are incorporated in their hybrid method using Attard's generalization [66] of the DH pair distribution functions. However, the influence of the ion-ion HIs on the viscosity, and on the relaxation mechanism part of the conductivity, are disregarded in their MCT-DDFT treatment. In related work, Dufreche *et al.* [62] have combined MCT and DDFT arguments with Kirkwood's friction formula for electrolyte friction to calculate the ion self-diffusion coefficients and velocity autocorrelation functions in a binary electrolyte solution. The finite ion sizes in this approach to self-diffusion are accounted for in MSA, and the inter-ion HIs are treated on the point-particle (Oseen) level of description. In [62], however, the effect of dynamic cross correlations in the intermediate scattering functions input is disregarded.

In a series of papers, using linear response theory we have developed a unifying MCT method for calculating linear conduction-diffusion [67, 68] and viscoelastic [68, 69] properties of non-dilute strong electrolyte solutions. This method builds on earlier work where a general MCT for the dynamic structure factor of Brownian particle mixtures with HIs has been developed [70–72]. Our statistical mechanical theory of electrolyte transport on the PM-GSmE level includes the influence of the solvent-mediated ion-ion HIs not only in the short-time response, but also in the relaxation mechanism contribution. It provides hereby a complete description of steady-state transport coefficients. This differentiates our method from earlier theoretical work where HIs were only incompletely considered, or where severe approximations such as the Nernst-Einstein relation between ion self-diffusion and conductivity have been invoked. Using a simplifying solution scheme, referred to as the MCT-HIs approach, easy-to-apply semi-analytic transport coefficient expressions have been derived and evaluated for an aqueous 1 : 1 strong electrolyte solution which is an overall electroneutral binary solution of monovalent cations and anions in water. The predicted coefficients for stick hydrodynamic BC on the PM ion surfaces agree well with experimental data for the electrolyte conductivity and viscosity, for ion concentrations extending even up to two molar. To analyze the dynamic influence of ion hydration shells, [68] includes a discussion on the significance of mixed stick-slip hydrodynamic surface boundary conditions, and on the effect of solvent permeability.

A thorough description of the MCT-HIs method with numerous numerical results is contained in [67–69]. To illustrate the method, Figs. 1 - 3 display additional results not included in the aforementioned papers. In Fig.

1, the MSA-HIs prediction of the molar conductivity Λ of an aqueous $1:1$ strong electrolyte solution is compared with experimental data for a $NaCl$ solution. The quantity Λ is the mean electric current density of ions per unit applied electric field strength, and per mol of salt unit. Results for mixed slip-stick BCs with three different hydrodynamic slip lengths, l_{slip}, are compared to each other. Here, l_{slip} is the distance into the interior of a PM ion for which the linear near-surface flow extrapolates to zero. The experimental conductivity data are overall well reproduced using the standard stick BC for which $l_{slip} = 0$, even though they are underestimated to some extent at large n_T. The agreement between theory and experiment becomes excellent for $l_{slip} = a/4$, a slip length compatible with the presence of ion hydration shells which are expected to cause some hydrodynamic slip. The slip length of an ion depends on the molecular structure and width of its hydration shell, and for a thicker shell also on the form of the local flow field which differs in character for electrophoresis and shear flow without external electric field. Fig. 1 depicts additionally theoretical results for the short-time (i.e. electrophoretic mechanism) part, Λ_S, of the conductivity, normalized by the electrolyte conductivity Λ_0 at infinite dilution. At larger n_T, the reduction of the conductivity by the relaxation mechanism becomes comparatively large to that caused by the short-time electrophoretic mechanism. As shown in [68], both the short-time and relaxation parts of Λ, and of the viscosity, are considerably affected by the HIs. At very low concentrations, the DFOF limiting law result for the conductivity is recovered by the MCT-HIs scheme.

Fig. 2 includes a MCT-HIs based analysis of the approximate Nernst-Einstein (NE) relation which links the conductivity to the ionic self-diffusion coefficients. For a symmetric $1:1$ electrolyte, the NE relation simply reads $\Lambda/\Lambda_0 \approx d_L/d_0$, where d_L is the long-time self-diffusion coefficient of the equally sized and equally valent anions and cations with common single-ion diffusion coefficient d_0. Owing to the neglected ion velocity cross correlations in the NE relation, the conductivity is severely overestimated by this relation.

Similar to the conductivity, the electrolyte viscosity η in excess to the solvent viscosity η_0, is given by the sum [69],

$$\Delta\eta_{exc} = \eta - \eta_0 = \Delta\eta_\infty + \Delta\eta \ ,$$

of a short-time (i.e. high-frequency) part $\Delta\eta_\infty$ and a shear-stress relaxation part $\Delta\eta$. The short-time part is of purely hydrodynamic origin and vanishes for point particles or when HIs are disregarded. Fig. 3 includes our MCT-HIs predictions for the excess viscosity of an aqueous $1:1$ electrolyte for values of the slip length as in Fig. 1, in comparison with the measured excess viscosity of $NaCl$ in water. The experimental data are well described by the MCT-HIs result when the standard stick BC is used. Usage of the slip length $l_{slip} = a/4$ results

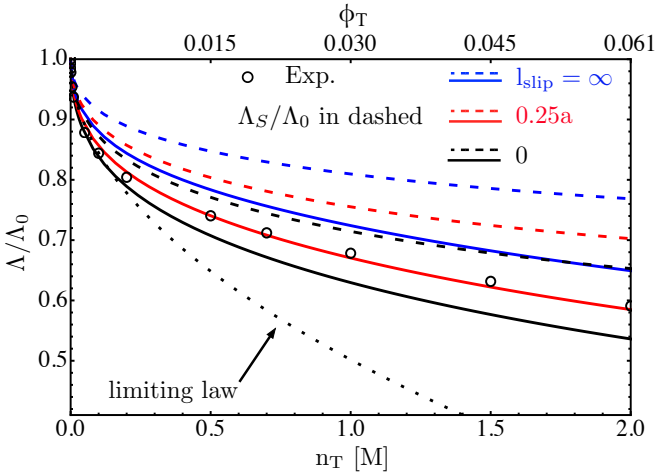

Figure 1. MCT-HIs based theoretical predictions for the normalized molar conductivity, Λ, of an aqueous $1:1$ electrolyte at $T = 25°$C (solid lines), for three hydrodynamic slip lengths as indicated. The corresponding short-time conductivity contributions, Λ_S, are shown as dashed lines. The hydrodynamic mean ion diameter, $\sigma = 2a = 4.58$Å, of hydrated Na^+ and Cl^- ions was used in the calculations. Open circles: experimental data for the molar conductivity of $NaCl$ dissociated in water, taken from [73]. Dotted line: DFOF limiting law result. The lower (upper) horizontal scale is for the total ion concentration n_T (total ion volume fraction ϕ_T).

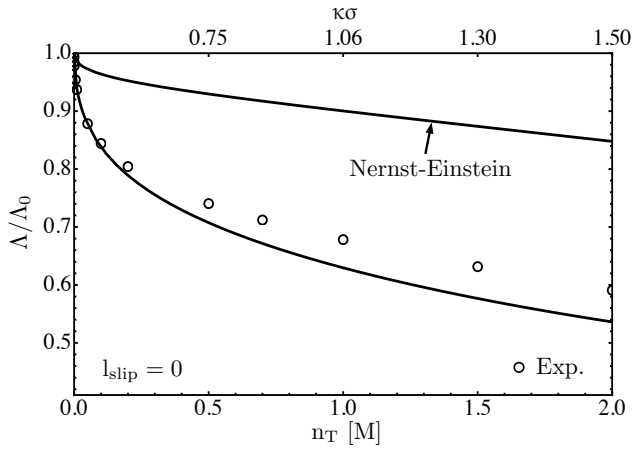

Figure 2. Accuracy check of the approximate Nernst-Einstein relation, $\Lambda/\Lambda_0 \approx d_L/d_0$, for the reduced molar conductivity of a symmetric aqueous $1:1$ electrolyte. Solid lines are simplified MCT-HIs results for d_L/d_0 (upper curve) and Λ/Λ_0 (lower curve), respectively, for zero slip length. All other system parameters are as in Fig. 1. Open circles: experimental conductivity data for $NaCl$ in water at $T = 25°$C [73].

however in a significant underestimation of the viscosity. This can be at least partially attributed to the fact that the mean local hydrodynamic environment of particles in shear flow is qualitatively different from the local environment in electrophoresis, with consequently different hydrodynamic slip lengths [67]. The strongest contribution

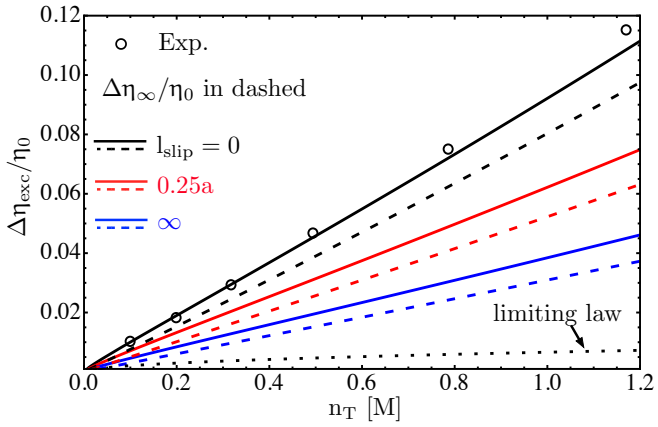

Figure 3. MCT-HIs based theoretical predictions for the concentration dependence of the reduced excess electrolyte viscosity, $\Delta\eta_{exc}/\eta_0$, of an aqueous 1 : 1 electrolyte at $T = 25°C$. Three hydrodynamic slip lengths are considered as indicated (solid lines), and $\sigma = 2a = 4.58$Å is used for the mean ion diameter. The corresponding reduced short-time viscosity contributions, $\Delta\eta_\infty$, are shown as dashed lines. Open circles: experimental data for the excess viscosity of $NaCl$ in water, taken from [74]. Dotted line: DFOF limiting law result (see [69]).

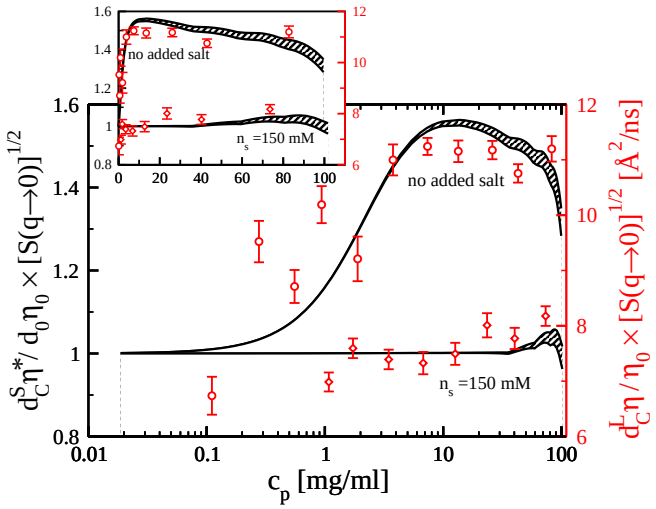

Figure 4. Experimental-theoretical test of the long-time and short-time KD-GSE relation with $\eta^* = \eta$ and $\eta^* = \eta_\infty$, respectively. Results for aqueous BSA solutions without added salt (upper data sets), and with 150 mM of added NaCl (lower data sets) are shown in their dependence on the protein concentration c_p. Red symbols: combination of d_C^L from DLS, η/η_0 from suspended couette rheometry, and $S(q \to 0)$ from static light scattering. Black lines: Theoretical results combining $d_C^S \approx d_C^L$ and η_∞, both calculated using the self-part corrected $\delta\gamma$ scheme [75], with $S(q \to 0)$ obtained from the MPB-RMSA scheme. For the long-time KD-GSE relation, $\eta = \eta_\infty + \Delta\eta$ has been used, with $\Delta\eta$ calculated using the MCT-HIs scheme. Lower boundaries of the theoretical curves correspond to the short-time KD-GSE relation, upper boundaries to the long-time version. The effective protein diameter is $\sigma = 7.40$ nm. Figure taken from [2].

to the steady-state viscosity is caused by the short-time viscosity part $\Delta\eta_\infty$. The limiting law regime, characterized by the $\sqrt{n_T}$ dependence of $\Delta\eta_{exc}$, is reached for very small concentrations only.

III. CROWDED GLOBULAR PROTEIN SOLUTIONS

There have been various attempts in the past to describe the collective diffusion in globular protein solutions using a simplifying colloid-type effective sphere model with Derjaguin-Landau-Verwey-Overbeek (DLVO)-like pair interactions. However, calculations of the collective diffusion coefficient d_C based on this model have been either quite approximate, in particular regarding the treatment of the protein HIs [76, 77], or restricted to the first-order correction in the volume fraction [78]. In a recent experimental-theoretical study, dynamic light scattering measurements of d_C and rheometric measurements of the steady-state viscosity η of crowded BSA solutions where compared with theoretical calculations based on an analytically treatable spheroid model of BSA with isotropic screened Coulomb interactions. For calculating the dynamic properties, easy-to-implement theoretical methods were used which account for the HIs [75]. The only input required by these methods is the colloidal static structure factor $S(q)$, obtained in [2] using the newly developed so-called MPB-RMSA integral equation scheme [79, 80]. All experimentally determined properties were reproduced theoretically with an at least semi-quantitative accuracy. In particular, the applicability range of the Kholodenko-Douglas generalized Stokes-Einstein (KD-GSE) relation [81],

$$\frac{d_C(\phi)\,\eta(\phi)}{d_0\,\eta_0}\sqrt{S(q\to 0,\phi)} = 1\,,$$

between collective diffusion coefficient, steady-state viscosity $\eta = \eta_\infty + \Delta\eta$ (with $\eta_\infty = \eta_0 + \Delta\eta_\infty$), and the square-root of the isothermal osmotic compressibility coefficient $S(q \to 0, \phi)$ was studied. The KD-GSE relation has been used in the biophysics and soft matter communities to deduce the viscosity from static and dynamic light scattering (SLS and DLS) data [82–84]. Note that the short-time (superscript S) and long-time (superscript L) forms of d_C are practically equal to each other, whereas $\eta_\infty < \eta$.

Fig. 4 provides a theoretical-experimental performance test of the short-time and long-time versions of the KD-GSE relation for BSA solutions at low salinity, i.e. $n_s = 1 - 3$ mM, and for the physiological salt concentration $n_s = 150$ mM. The experimental data agree overall well with the theoretical predictions. For low salinity and larger protein concentrations c_p, pronounced deviations from the protein concentration independent value one of

the KD-GSE relation are observed. A pronounced violation of this relation is predicted theoretically also for suspensions of large charge-stabilized colloidal spheres. For neutral hard-sphere suspensions up to $\phi \lesssim 0.4$, the KD-GSE relation is, however, decently well fulfilled [75]. An effective charged-sphere model analysis similar to that for BSA was made in a joint experimental-theoretical study of suspensions of charged gibbsite platelets (with aspect ratio 1 : 11) in the isotropic liquid phase [85]. As shown in this work, the effect of translation-rotation interparticle coupling (disregarded in the effective sphere treatment) is less pronounced for collective diffusion, but it is particularly strong for translational and rotational self-diffusion at larger concentrations.

IV. CONCENTRATED CHARGE-STABILIZED COLLOIDAL SUSPENSIONS

We commence this section by shortly summarizing recent progress made in developing computer simulation and numerical schemes allowing to quantify microion electrokinetic effects on transport properties of charge-stabilized suspensions at non-zero concentrations. In the smoothed profile method (SMP) of Yamamoto, Nakayama and Kim [86, 87], and in the related fluid particle dynamics (FPD) method of Tanaka and Araki [88], the solvent and the microions are treated as continuous fields, like in the SET approach. Only the colloidal macroions are treated explicitly as particles, i.e. as high-viscosity liquid droplets in FPD, and as particles with a smoothed interface to the solvent in SMP. The particles in both methods act on the solvent through continuous body forces rather than through moving boundaries. This simplification results in efficient numerical solution schemes suitable for concentrated suspensions. The advantage of the SMP method is that larger time increments can be selected. Since the microions in both methods are described in a mean-field way, local charge ordering effects beyond the Poisson-Boltzmann (PB) level are not considered. Both methods have been applied in particular to colloidal electrophoresis. The electrophoretic mobility results by the SMP method [86] are similar to those obtained by SET spherical cell model calculations where overlapping colloidal EDLs are approximately accounted for [25]. Giupponi and Pagonabarraga solve the (non-linearized) SET equations by a discretized lattice Boltzmann (LB) formulation of the solvent, coupled to the colloid surface grid points by kinetic bounce-back rules, and combined with a solver of the correspondingly discretized SET convection-diffusion equations for the microion densities [89]. They could show that for microion Peclet numbers $\gtrsim 0.3$ where flow advection becomes comparably important to single-microion diffusion, non-linear microion advection enhances the electrophoretic mobility.

Lobaskin, Dünweg and collaborators [92, 93] have developed a hybrid simulation method where the microions are considered explicitly, and where the raspberry-like macroion model surface is coupled through a friction term to a LB background describing the Navier-Stokes hydrodynamics of a structureless solvent. While this simulation method includes microion correlations beyond the PB level, the price to pay is a larger numerical effort. Due to the more costly numerics, only the electrophoresis of a single macroion plus its neutralizing microion cloud in a box with periodic BCs has been considered so far. Non-zero colloid concentration effects are accounted for, akin to standard cell model calculations, by adjusting the box to macroion size ratio to the given volume fraction. A similar Molecular Dynamics - LB hybrid simulation method was used by Chatterji and Horbach to analyze the nature of the effective electrophoretic macroion charge in single-colloid electrophoresis [94]. To describe electrophoresis of a spherical macroion in a finite box on level of the mean-field SET equations, Dünweg *et al.* have developed a numerically efficient solver [95], and they have used in addition the finite-element software package COMSOL [96].

Except for electrophoresis and sedimentation, microionic electrokinetic contributions to linear colloidal transport coefficients are secondary effects in magnitude, in particular for suspensions of strongly correlated charged colloidal particles. Using a simplified MCT-HIs method, this has been shown quantitatively in [97, 98] for the long-time colloidal self-diffusion coefficient. In the remainder of this section, we discuss colloidal diffusion properties and the viscosity of concentrated suspensions, which are well described on basis of the OMF model of microion-dressed macroions. In this model, colloidal dynamic properties can be obtained to high accuracy using the accelerated Stokesian Dynamics (ASD) simulation method for charge-stabilized Brownian spheres [1, 75, 99, 100] which fully accounts for the colloid HIs including lubrication interactions. It was used so far mainly for the calculation of short-time diffusion properties of charge-stabilized colloids, giving results in quantitative agreement with dynamic scattering data (see [100, 101] for an elaborate comparison). Recently, (A)SD results have been obtained also for long-time diffusion transport coefficients, and for self-intermediate and collective dynamic scattering functions [102].

We mention here in addition the powerful hydrodynamic force multipole simulation method by Cichocki, Ekiel-Jezewska, Wajnryb and coworkers [103], encoded in the HYDROMULTIPOLE program, which allows for an easy implementation of different hydrodynamic particle models. The method has been used for a comprehensive simulation study of short-time dynamic properties of suspensions of solvent-permeable hard spheres, with uniform permeability [90, 104, 105], and also with internal core-shell structure [106]. The flow inside the permeable region of a particle is described by the Brinkman-Debye-Bueche fluid model. Results have been discussed including the high-frequency viscosity η_∞, and the hydrodynamic function $H(q)$. The latter quantity reduces

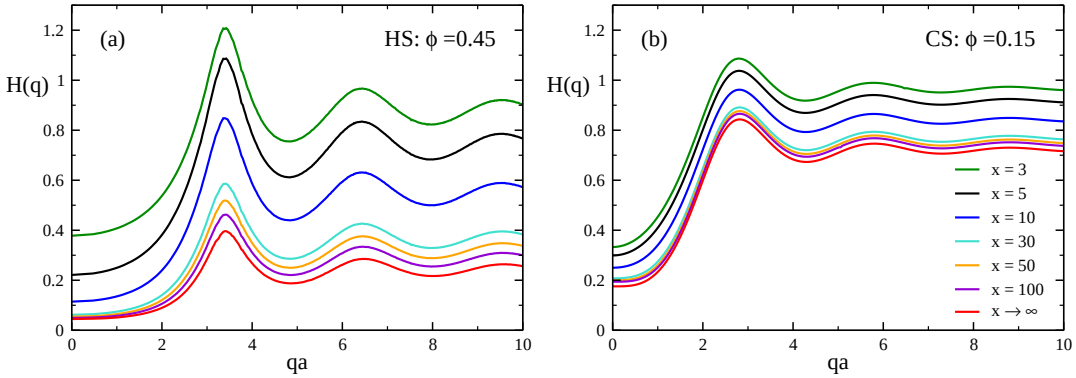

Figure 5. Wavenumber-dependent hydrodynamic function $H(q)$, of solvent-permeable colloidal spheres, with values of the inverse permeability coefficient x and volume fraction ϕ as indicated. Small x correspond to large, and large x to small permeabilities. (a) Simulation results for uncharged hard spheres taken from [90]. The curve for stick hydrodynamic BC ($x = \infty$) agrees with the ASD simulation data. (b) Analytic results for charged spheres of diameter $2a = 200$ nm and effective particle charge number $Z = 200$, immersed in a 0.5 mM 1 : 1 aqueous electrolyte solution with Bjerum length $L_B = 7.11$ nm. The charged spheres interact by a screened Coulomb potential of DLVO type. The results in (b) were obtained by a pairwise additive HIs approach, with truncated pair mobilities of $\mathcal{O}\left(1/r^7\right)$ in the pair distance r taken from [91], and using the accurate MPB-RMSA static structure factor input.

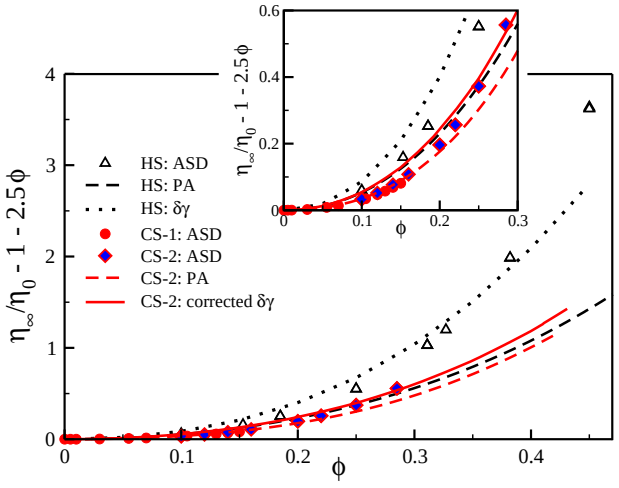

Figure 6. Reduced high-frequency viscosity, η_∞/η_0, as function of ϕ, for a neutral hard-sphere suspension (HS, in black), and two deionized charged-sphere suspensions (CS-1 and CS-2, in red). The leading-order Einstein viscosity contribution, $1 + 2.5\phi$, is subtracted to expose the differences. Symbols: ASD simulation results. Dashed lines: PA-approximation results. Dotted lines: $\delta\gamma$-scheme results. Solid lines: self-part corrected $\delta\gamma$-scheme results. All analytic schemes use the MPB-RMSA $S(q)$ as input. The CS-1 results represented by red filled circles are ASD data for $L_B = 5.617$ nm, $\sigma = 200$ nm, and $Z = 100$. The ASD data for the more weakly charged and smaller particles of system CS-2, where $L_B = 0.71$ nm, $\sigma = 50$ nm, and $Z = 70$, are indicated by red diamonds filled in blue. The parameters of system CS-2 have been used in the analytic calculations. The inset magnifies details at lower ϕ. Figure taken from [75].

to the normalized mean sedimentation velocity for small wavenumber q, and to the short-time self-diffusion coefficient d_S for large q.

HYDROMULTIPOLE results for the $H(q)$ of a concentrated suspension of solvent-permeable, i.e. porous, hard spheres of excluded volume radius a are depicted in Fig. 5(a), for various values of the inverse permeability coefficient $x = a/l_{perm}$. Here, l_{perm} is the hydrodynamic penetration depth. As it is noticed, (short-time) self- and collective diffusion, and sedimentation, are significantly enhanced with increasing solvent-permeability of the particles. The high-frequency viscosity, on the other hand, is lowered. In [104], it is shown through comparison with precise HYDROMULTIPOLE simulation data for η_∞ that the cell model approach for permeable and non-permeable spheres [107] gives rather poor predictions for the concentration dependence of η_∞.

The force multipole method by Chichocki and collaborators has been applied so far to electrically neutral solvent-permeable colloids only. At lower ϕ, however, non-pairwise additive HIs contributions are small for charged particles due to their longer range mutual repulsion. These contributions can thus be neglected to a decent approximation. Fig. 5(b) shows new hydrodynamic function results for permeable charged spheres, which we have obtained using truncated two-sphere hydrodynamic mobility tensors in combination with the MPB-RMSA static structure factor input. According to the figure, the influence of solvent permeability on $H(q)$ is substantially weaker for charged colloidal particles.

In elaborate studies, it has been shown that the ASD simulation results for short-time diffusion properties of charge-stabilized spheres with stick hydrodynamic BC, and a large body of experimental data alike [100, 101], are well reproduced, for a broad range of interaction

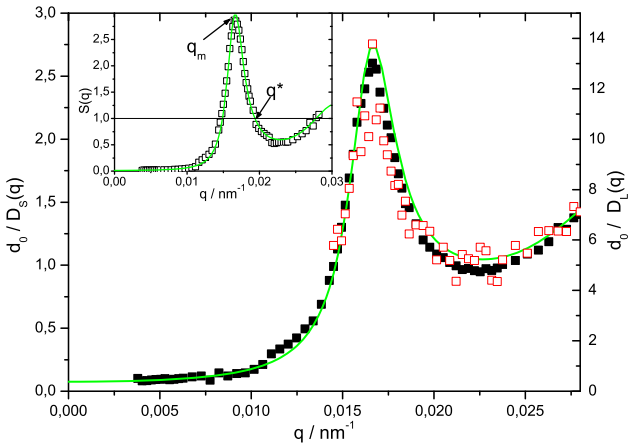

Figure 7. Dynamic light scattering results for the normalized inverse short-time diffusion function $d_0/D_S(q)$ (filled black squares, scale on left side) and inverse long-time diffusion function $d_0/D_L(q)$ (open red squares, scale on right side) of charge-stabilized silica spheres at $\phi = 0.14$. Solid curve: theoretical prediction by the $\delta\gamma$-scheme for the wavenumber dependence of $d_0/D_S(q)$, using the MPB-RMSA input for $S(q)$ shown in the inset together with the experimental data. Figure taken from [110].

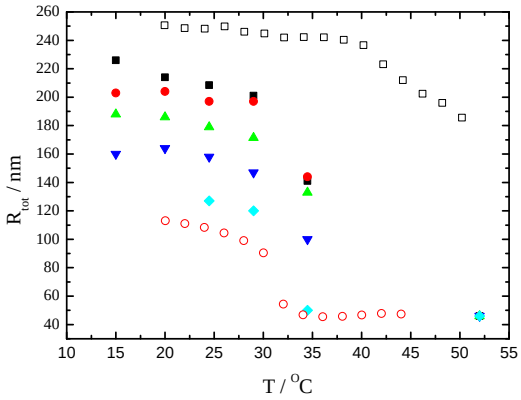

Figure 8. Outer radius, R_{tot}, as a function of T for ionic PNiPAm dispersions (filled symbols) at microgel particle concentration $n_p = 0.0053$ (black squares), 0.0074 (red circles), 0.013 (green upper triangles), 0.022 (blue lower triangles) and 0.069 M (light blue diamonds). Open symbols: Results for a dilute particle solutions with $n_p = 0.1$ nM and pH = 6.3 (black), and pH = 3.0 (red). Figure taken from [115].

parameters and volume fractions typical of the liquid-phase state, using the analytic and easy-to-implement $\delta\gamma$ method by Beenakker and Mazur, amended by an improved (i.e., "corrected") self-part contribution [75]. Makuch and Cichocki [108] have critically assessed the approximations going into the Beenakker-Mazur method. Their revised version of the $\delta\gamma$ method which includes an improved hydrodynamic mobility matrix input leads overall to larger differences from the hard-sphere simulation data. This points to a fortuitous cancellation of errors introduced by the approximations going into the original Beenakker-Mazur method.

A self-part corrected version of the $\delta\gamma$ method has been successfully used in addition for the calculation of the high-frequency viscosity of charge-stabilized colloids at lower salinity. Results by this method are shown in Fig. 6, and compared with ASD simulation results for charge-stabilized spheres (CS) and neutral hard spheres (HS) with stick hydrodynamic BC. Also included are viscosity results obtained using numerically accurate values for the full pairwise-additive two-sphere hydrodynamic mobilities including lubrication forces. This is referred to as the PA-approximation. While $\eta_\infty$is for CS smaller than for HS, the opposite ordering is valid in general for the steady-state, low-shear rate viscosity η, owing to the for CS substantially larger colloidal shear-stress relaxation contribution $\Delta\eta$. Possible correlations between η and η_∞, and the Debye screening length and macroion electric surface potential, are discussed in [109] on basis of theories for semidilute systems with and without single-colloid electrokinetics included.

A dynamic scaling relation for the normalized dynamic structure factor,

$$S(q,t)/S(q) \approx \exp\left\{-q^2\,\frac{D_S(q)}{d_S}\,W(t)\right\}\ ,$$

has been shown in [110] to apply approximately to charge-stabilized colloids, within the experimentally accessed correlation time window, and for scattering wavenumbers q around the position, q_m, of the principal static structure factor peak. Here, $W(t) = \langle \Delta r^2\,(t)\rangle\,/6$ is the particle mean-squared displacement with short-time slope d_S, and $D_S(q) = d_0\,H(q)/S(q)$ is the short-time diffusion function. The scaling relation was initially found empirically by Segrè and Pusey for the case of colloidal hard spheres [111] (see here also the MCT study of Fuchs and Mayr [112]). It implies in particular that $D_L(q)/D_S(q) \approx d_L/d_S$, for values of q near to q_m. Here, $D_L(q)$ denotes the relaxation rate of the long-time decay of $S(q,t)$ which in the experimental time window is single-exponential, and d_L is the colloidal long-time self-diffusion coefficient which is smaller than d_S. Fig. 7 demonstrates that this relation is indeed valid to a decent approximation for charge-stabilized spheres. The validity of the time-wavenumber factorization scaling of $S(q,t)$ has been repeatedly challenged, also for the reason that the true long-time regime can hardly be reached experimentally [113, 114]). As it was argued already in [110], from a theoretical viewpoint dynamic scaling is merely an approximate feature. This viewpoint is corroborated by a recent study, where Stokesian dynamics, Brownian dynamics, and MCT calculations of $S(q,t), W(t)$ and $D_S(q)$ have been compared [102].

Ionic microgels belong to the subclass of ultra-soft colloids where the effective interaction potential crosses

over from a screened Coulomb repulsion at non-overlap distances to a smoothly increasing repulsion of finite interaction energy for overlapping particles [116, 117]. A fraction of the counterions released by ionic polymer backbone groups of the microgel network is confined to the interior of the ionic microgel particles, affecting therefore their swelling behavior through the microion osmotic pressure difference. A comprehensive experimental-theoretical study of the concentration- and temperature dependent swelling behavior of PNiPAm ionic core-shell microgel particles was made in [115]. Results by this study for the outer microgel radius R_{tot}, deduced as a function of microgel number density n_p and temperature T, are included in Fig. 8. In the theoretical part of the study, state-of-the art analytic OMF methods discussed also in relation to Figs. 4 - 7 have been used. Fig. 8 highlights in particular the strong concentration dependence of the (outer) microgel radius in the non-collapsed microgel state at lower temperatures.

V. CONCLUSIONS

We have reviewed recent advances in our understanding of linear diffusion-convection and viscoelastic transport properties of dispersions of charged Brownian particles. Various theoretical and computer simulation methods have been discussed and compared. Regarding the electrokinetics of electrolyte solutions, a fast and versatile simplified MCT-HIs method is now available, making predictions in good agreement with experimental data. With some effort, this method can be extended to frequency-dependent transport properties, and to size- and charge-asymmetric electrolytes. Work on these extensions is in progress. The MCT-HIs method keeps promise to tackle also the electrophoresis and conductivity of colloidal macroions and globular proteins with overlapping EDLs. The microions are hereby treated on equal footing with the macroions, both statically and dynamically. While great progress has been made in the development of numerical cell model and simulation schemes describing colloidal electrokinetics, the proper inclusion of electro-steric and hydrodynamic aspects of the microion dynamics beyond the mean-field level is still a challenging task, in particular for concentrated suspensions. A detailed evaluation of the pros and cons of the various existing simulation schemes for selected colloidal electrophoresis benchmark problems is still on demand. Short-time dynamic properties treated on the level of the OMF model are meanwhile well understood, thanks to detailed experimental and (A)SD simulation results. Well-tested accurate theoretical methods for calculating short-time dynamic properties such as the self-part corrected $\delta\gamma$ scheme are now available. They allow for a fast analysis of experimental data covering a broad range of system parameters. Short-time dynamic properties are of relevance not only in their own right but are required also as input to theories describing colloidal long-time dynamics in concentrated systems such as MCT and DDFT approaches, and their hybrids. A lot remains to be learned about the long-time dynamics of charge-stabilized suspensions and globular protein solutions, in particular when macroions with internal electrosteric and hydrodynamic structure are considered.

acknowledgement

We thank G. Abade, B. Cichocki, J. Dhont, S. Egelhaaf, M. Ekiel-Jezewska, J. Gapinksi, Ch. Gögelein, P. Holmqvist, K. Makuch, M. McPhie, P.S. Mohanty, T. Palberg, A. Patkowski, J. Riest, R. Roa, F. Schreiber, P. Schurtenberger, and E. Wajnryb for helpful discussions and fruitful collaborations. Financial support by the Deutsche Forschungsgemeinschaft (SFB-TR6, Project B2) is gratefully acknowledged.

Abbreviations:

ASD	Accelerated Stokesian Dynamics.
BSA	Bovine serum albumin.
BCs	Boundary conditions.
CS	Charged spheres.
DDFT	Dynamic density functional theory.
DFOF	Debye-Falkenhagen-Onsager-Fuoss.
DH	Debye-Hückel.
DLS	Dynamic light scattering.
DLVO	Derjaguin-Landau-Verwey-Overbeek.
EDLs	Electric double layers.
FPD	Fluid particle dynamics.
GSmE	Generalized Smoluchowski equation.
HIs	Hydrodynamic interactions.
HNC	Hypernetted chain.
HS	Uncharged, pairwise additive hard spheres.
KD-GSE	Kholodenko-Douglas generalized Stokes-Einstein (relation).
LB	Lattice-Boltzmann.
MCT	Mode-coupling theory.
MPB-RMSA	Modified penetrating background-corrected rescaled mean spherical approximation.
MSA	Mean spherical approximation.
NE	Nernst-Einstein.
OMF	One-component macroion fluid.
PB	Poisson-Boltzmann.
PM	Primitive model.
PNiPAm	Poly (N-isopropylacrylamide).
SET	Standard electrokinetic theory.
SLS	Static light scattering.
SMP	Smoothed profile method.

[1] J. Gapinski, A. Wilk, A. Patkowski, W. Häußler, A. J. Banchio, R. Pecora, and G. Nägele, J. Chem. Phys. **123**, 054708 (2005).

[2] M. Heinen, F. Zanini, F. Roosen-Runge, D. Fedunova, F. Zhang, M. Hennig, T. Seydel, R. Schweins, M. Sztucki, M. Antalik, F. Schreiber, and G. Nägele, Soft Matter **8**, 1404 (2012).

[3] F. Roosen-Runge, M. Hennig, F. Zhang, R. M. J. Jacobs, M. Sztucki, H. Schober, T. Seydel, and F. Schreiber, Proc. Natl. Acad. Sci. U.S.A. **108**, 11815 (2011).

[4] C. Gögelein, G. Nägele, R. Tuinier, T. Gibaud, A. Stradner, and P. Schurtenberger, J. Chem. Phys. **129**, 085102 (2008).

[5] S. U. Egelhaaf, V. Lobaskin, H. H. Bauer, H. P. Merkle, and P. Schurtenberger, Eur. Phys. J. E **13**, 153 (2004).

[6] C. Gögelein, D. Wagner, F. Cardinaux, G. Nägele, and S. U. Egelhaaf, J. Chem. Phys. **136**, 015102 (2012).

[7] M. E. Davis, J. D. Madura, J. Sines, B. A. Luty, S. A. Allison, and J. A. Mccamon, Methods in Enzymology **202**, 473 (1991).

[8] W. Nonner, D. P. Chen, and B. Eisenberg, J. Gen. Physiol. **113**, 773 (1999).

[9] H. D. B. Jenkins and Y. Marcus, Chem. Rev. **95**, 2695 (1995).

[10] P. G. Wolynes, Annu. Rev. Phys. Chem. **31**, 345 (1980).

[11] J. M. G. Barthel, H. Krienke, and W. Kunz, *Physical Chemistry of Electrolyte Solutions*, Topics in Physical Chemistry, Vol. 5 (Steinkopff, Darmstadt, 1998).

[12] H. Falkenhagen and W. Ebeling, "Theorie der Elektrolyte," S. Hirzel Verlag, Stuttgart (1971).

[13] G. Nägele, in *In: Physics of Complex Colloids - Proceedings of International School of Physics Enrico Fermi*, edited by C. Bechinger, F. Sciortino, and P. Ziherl (IOS Amsterdam; SIF Bologna, 2013).

[14] H. Ohshima, *Theory of Colloid and Interfacial Electric Phenomena*, Interface Science and Technology, Vol. 12 (Elsevier Academic Press, Amsterdam, 2006).

[15] J. H. Masliyah and S. Bhattacharjee, *Electrokinetic and Colloid Transport Phenomena* (Johns Wiley & Sons, Hoboken, New Jersey, 2006).

[16] M. Z. Bazant, M. S. Kilic, B. D. Storey, and A. Ajdari, Adv. Colloid Interface Sci. **152**, 48 (2009).

[17] A. S. Khair and T. M. Squires, J. Fluid. Mech. **640**, 343 (2009).

[18] R. Roa, F. Carrique, and E. Ruiz-Reina, Phys. Chem. Chem. Phys. **13**, 19437 (2011).

[19] J. J. Lopez-Garcia, M. J. Aranda-Rascon, C. Grosse, and J. Horno, J. Colloid Interface Sci. **356**, 325 (2011).

[20] M. Lozada-Cassou, E. Gonzales-Tovar, and W. Olivares, Phys. Rev. E **60**, R17 (1999).

[21] M. Lozada-Cassou and E. González-Tovar, J. Colloid Interface Sci. **239**, 285 (2001).

[22] M. Lozada-Cassou and E. González-Tovar, J. Colloid Interface Sci. **240**, 644 (2001).

[23] H. Manzanilla-Granados, F. Jimenez-Angeles, and M. Lozada-Cassou, Colloids Surf. A **376**, 59 (2011).

[24] F. Carrique, F. J. Arroyo, and A. V. Delgado, Colloids Surf. A **195**, 157 (2001).

[25] F. Carrique, J. Cuquejo, F. J. Arroyo, M. L. Jiménez, and A. V. Delgado, Adv. Colloid Interface Sci. **118**, 43 (2005).

[26] C. P. Chiang, E. Lee, Y. Y. He, and J. P. Hsu, J. Phys. Chem. B **110**, 1490 (2006), http://pubs.acs.org/doi/pdf/10.1021/jp054969r.

[27] J. M. Ding and H. J. Keh, J. Colloid Interface Sci. **236**, 180 (2001).

[28] M. W. Kozak and E. J. Davis, J. Colloid Interface Sci. **127**, 497 (1989).

[29] M. W. Kozak and E. J. Davis, J. Colloid Interface Sci. **129**, 166 (1989).

[30] S. Levine and G. H. Neale, J. Colloid Interface Sci. **47**, 520 (1974).

[31] H. Ohshima, J. Colloid Interface Sci. **188**, 481 (1997).

[32] H. Ohshima, J. Colloid Interface Sci. **229**, 140 (2000).

[33] V. N. Shilov, N. I. Zharkikh, and Y. B. Borkovskaya, Colloid J. - USSR **43**, 434 (1981).

[34] E. K. Zholkovskiy, J. H. Masliyah, V. N. Shilov, and S. Bhattacharjee, Adv. Colloid Interface Sci. **134**, 279 (2007).

[35] E. K. Zholkovskiy, V. N. Shilov, J. H. Masliyah, and M. P. Bondarenko, Can. J. Chem. Eng. **85**, 701 (2007).

[36] T. Vissers, A. Imhof, F. Carrique, A. V. Delgado, and A. van Blaaderen, J. Colloid Interface Sci. **361**, 443 (2011).

[37] J. P. Hsu, E. Lee, and F. Y. Yen, J. Chem. Phys. **112**, 6404 (2000).

[38] J. J. Lopez-Garcia, C. Grosse, and J. Horno, J. Colloid Interface Sci. **301**, 651 (2006).

[39] S. Ahuali, M. L. Jiménez, F. Carrique, and A. V. Delgado, Langmuir **25**, 1986 (2009).

[40] J. Ennis and L. R. White, J. Colloid Interface Sci. **185**, 157 (1997).

[41] J. Ennis and L. R. White, J. Colloid Interface Sci. **189**, 382 (1997).

[42] A. A. Shugai, S. L. Carnie, D. Y. C. Chan, and J. L. Anderson, J. Colloid Interface Sci. **191**, 357 (1997).

[43] T. Palberg, T. Köller, B. Sieber, H. Schweinfurth, H. Reiber, and G. Nägele, J. Phys.: Condens. Matter **24**, 464109 (2012).

[44] L. Onsager and R. M. Fuoss, J. Phys. Chem. - US **36**, 2689 (1932).

[45] L. Onsager and S. K. Kim, J. Phys. Chem. - US **61**, 215 (1957).

[46] L. Onsager, Ann. N.Y. Acad. Sci. **46**, 241 (1945).

[47] H. Falkenhagen and E. L. Vernon, Phil. Mag. S. 7 **14**, 537 (1932).

[48] W. Ebeling, R. Feistel, G. Kelbg, and R. Sandig, J. Non-Eq. Thermod. **3**, 11 (1978).

[49] D. Kremp, W. Ebeling, H. Krienke, and R. Sändig, J. Stat. Phys. **33**, 99 (1983).

[50] O. Bernard, W. Kunz, P. Turq, and L. Blum, J. Phys. Chem. - US **96**, 3833 (1992).

[51] S. Durand-Vidal, P. Turq, O. Bernard, C. Treiner, and L. Blum, Physica A **231**, 123 (1996).
[52] S. Durand-Vidal, P. Turq, and O. Bernard, J. Phys. Chem. - US **100**, 17345 (1996).
[53] J. F. Dufreche, O. Bernard, S. Durand-Vidal, and P. Turq, J. Phys. Chem. B **109**, 9873 (2005).
[54] G. M. Roger, S. Durand-Vidal, O. Bernard, and P. Turq, J. Phys. Chem. B **113**, 8670 (2009).
[55] L. Blum and J. S. Høye, J. Phys. Chem. **81**, 1311 (1977).
[56] K. Hiroike, Mol. Phys. **33**, 1195 (1977).
[57] O. Bernard, W. Kunz, P. Turq, and L. Blum, J. Phys. Chem. - US **96**, 398 (1992).
[58] J. F. Dufreche, O. Bernard, and P. Turq, J. Chem. Phys. **116**, 2085 (2002).
[59] J. F. Dufreche, O. Bernard, and P. Turq, J. Mol. Liq. **118**, 189 (2005).
[60] B. U. Felderhof, J. Chem. Phys. **118**, 8114 (2003).
[61] J. F. Dufreche, O. Bernard, M. Jardat, and P. Turq, J. Chem. Phys. **118**, 8116 (2003).
[62] J. F. Dufreche, M. Jardat, P. Turq, and B. Bagchi, J. Phys. Chem. B **112**, 10264 (2008).
[63] A. Chandra and B. Bagchi, J. Chem. Phys. **110**, 10024 (1999).
[64] A. Chandra and B. Bagchi, J. Phys. Chem. B **104**, 9067 (2000).
[65] A. Chandra and B. Bagchi, J. Chem. Phys. **113**, 3226 (2000).
[66] P. Attard, Phys. Rev. E **48**, 3604 (1993).
[67] C. Contreras-Aburto and G. Nägele, J. Chem. Phys., accepted (2013).
[68] C. Contreras-Aburto and G. Nägele, J. Chem. Phys., accepted (2013).
[69] C. Contreras-Aburto and G. Nägele, J. Phys.: Condens. Matter **24**, 464108 (2012).
[70] G. Nägele and J. K. G. Dhont, J. Chem. Phys. **108**, 9566 (1998).
[71] G. Nägele and J. Bergenholtz, J. Chem. Phys. **108**, 9893 (1998).
[72] G. Nägele, J. Bergenholtz, and J. K. G. Dhont, J. Chem. Phys. **110**, 7037 (1999).
[73] D. G. Miller, J. Phys. Chem. - US **70**, 2639 (1966).
[74] D. J. P. Out and J. M. Los, J. Solution Chem. **9**, 19 (1980).
[75] M. Heinen, A. J. Banchio, and G. Nägele, J. Chem. Phys. **135**, 154504 (2011).
[76] W. Bowen and A. Mongruel, Colloids Surf. A **138**, 161 (1998).
[77] Y. X. Yu, A. W. Tian, and G. H. Gao, Phys. Chem. Chem. Phys. **7**, 2423 (2005).
[78] P. Prinsen and T. Odijk, J. Chem. Phys. **127**, 115102 (2007).
[79] M. Heinen, P. Holmqvist, A. J. Banchio, and G. Nägele, J. Chem. Phys. **134**, 044532 (2011).
[80] M. Heinen, P. Holmqvist, A. J. Banchio, and G. Nägele, J. Chem. Phys. **134**, 129901 (2011).
[81] A. L. Kholodenko and J. F. Douglas, Phys. Rev. E **51**, 1081 (1995).
[82] F. Nettesheim, M. W. Liberatore, T. K. Hodgdon, N. J. Wagner, E. W. Kaler, and M. Vethamuthu, Langmuir **24**, 7718 (2008).
[83] A. K. Gaigalas, V. Reipa, J. B. Hubbard, J. Edwards, and J. Douglas, Chem. Eng. Sci. **50**, 1107 (1995).
[84] D. E. Cohen, G. M. Thurston, R. A. Chamberlin, G. B. Benedek, and M. C. Carey, Biochemistry **37**, 14798 (1998).
[85] D. Kleshchanok, M. Heinen, G. Nägele, and P. Holmqvist, Soft Matter **8**, 1584 (2012).
[86] K. Kim, Y. Nakayama, and R. Yamamoto, Phys. Rev. Lett. **96**, 208302 (2006).
[87] E. Yamamoto, Y. Nakayama, and K. Kim, Int. J. Mod. Phys. C **20**, 1457 (2009).
[88] T. Araki and H. Tanaka, Europhys. Lett. **82**, 18004 (2008).
[89] G. Giupponi and I. Pagonabarraga, Phys. Rev. Lett. **106**, 248304 (2011).
[90] G. C. Abade, B. Cichocki, M. L. Ekiel-Jezewska, G. Nägele, and E. Wajnryb, J. Chem. Phys. **132**, 014503 (2010).
[91] P. Reuland, B. U. Felderhof, and R. B. Jones, Physica A **93**, 465 (1978).
[92] V. Lobaskin, B. Dünweg, and C. Holm, J. Phys.: Condens. Matter **16**, S4063 (2004).
[93] V. Lobaskin, B. Dünweg, B. Medebach, T. Palberg, and C. Holm, Phys. Rev. Lett. **98**, 176105 (2007).
[94] A. Chatterji and J. Horbach, J. Phys.: Condens. Matter **22**, 494102 (2010).
[95] R. Schmitz and B. Dünweg, J. Phys.: Condens. Matter **24**, 464111 (2012).
[96] B. Dünweg, V. Lobaskin, K. Seethalakshmy-Hariharan, and C. Holm, J. Phys.: Condens. Matter **20**, 404214 (2008).
[97] M. G. McPhie and G. Nägele, J. Chem. Phys. **127**, 034906 (2007).
[98] M. G. McPhie and G. Nägele, J Phys-Condens Mat **16**, S4021 (2004).
[99] A. J. Banchio and G. Nägele, J. Chem. Phys. **128**, 104903 (2008).
[100] M. Heinen, P. Holmqvist, A. J. Banchio, and G. Nägele, J. Appl. Cryst. **43**, 970 (2010).
[101] F. Westermeier, B. Fischer, W. Roseker, G. Grübel, G. Nägele, and M. Heinen, J. Chem. Phys. **137**, 114504 (2012).
[102] A. J. Banchio, P. Holmqvist, M. Heinen, and G. Nägele, (2013), submitted.
[103] B. Cichocki, B. U. Felderhof, K. Hinsen, E. Wajnryb, and J. Blawzdziewicz, J. Chem. Phys. **100**, 3780 (1994).
[104] G. C. Abade, B. Cichocki, M. L. Ekiel-Jezewska, G. Nägele, and E. Wajnryb, J. Phys.: Condens. Matter **22**, 322101 (2010).
[105] G. C. Abade, B. Cichocki, M. L. Ekiel-Jezewska, G. Nägele, and E. Wajnryb, J. Chem. Phys. **133**, 084906 (2010).
[106] G. C. Abade, B. Cichocki, M. L. Ekiel-Jezewska, G. Nägele, and E. Wajnryb, J. Chem. Phys. **136**, 104902 (2012).
[107] H. Ohshima, Colloids Surf. A **347**, 33 (2009).
[108] K. Makuch and B. Cichocki, J. Chem. Phys. **137**, 184902 (2012).
[109] W. B. Russel, Ind. Eng. Chem. Res. **48**, 2380 (2009).
[110] P. Holmqvist and G. Nägele, Phys. Rev. Lett. **104**, 058301 (2010).
[111] P. N. Segrè and P. N. Pusey, Phys. Rev. Lett. **77**, 771 (1996).
[112] M. Fuchs and M. R. Mayr, Phys. Rev. E **60**, 5742 (1999).
[113] L. B. Lurio, D. Lumma, A. R. Sandy, M. A. Borthwick, P. Falus, S. G. J. Mochrie, J. F. Pelletier, M. Sutton, L. Regan, A. Malik, and G. B. Stephenson, Phys. Rev. Lett. **84**, 785 (2000).

[114] V. A. Martinez, J. H. J. Thijssen, F. Zontone, W. van Megen, and G. Bryant, J. Chem. Phys. **134**, 054505 (2011).
[115] P. Holmqvist, P. S. Mohanty, G. Nägele, P. Schurtenberger, and M. Heinen, Phys. Rev. Lett. **109**, 048302 (2012).
[116] A. R. Denton, Phys. Rev. E **67**, 011804 (2003).
[117] C. N. Likos, "Structure and thermodynamics of ionic microgels, in: Microgel suspensions: Fundamentals and applications," (Wiley-VCH Verlag GmbH & Co. KGaA, 2011) Chap. 7.